



The Analysis of the Spatio-temporal Evolution of the Heat Island Effect and its Influencing Factors in Huadu District, Guangzhou

Bingyi Li¹, Ruei-Yuan Wang^{2,*}

^{1,2}School of Sciences, Guangdong University of Petrochem Technology (GDUPT), Maoming 525000, China (Corresponding author: Ruei-Yuan Wang PhD)

Received: 25 Feb 2024; Received in revised form: 04 Apr 2024; Accepted: 12 Apr 2024; Available online: 22 Apr 2024

©2024 The Author(s). Published by Infogain Publication. This is an open access article under the CC BY license (<https://creativecommons.org/licenses/by/4.0/>).

Abstract— This study aims to explore the urban heat island intensity and change characteristics of Huadu District, Guangzhou. Landsat 8 was used as the data source, and an atmospheric transmission model was used to invert the surface temperature of Huadu District, Guangzhou, in winter 2013 and 2021, extract the urban core area, and divide the heat island effect area. The results show that the urban heat island of Huadu District in Guangzhou has changed greatly in 2021. Compared with 2013, the proportion of low-temperature areas and sub-low temperature areas in urban areas has decreased in 2021, while the high-temperature area, sub-low temperature area, and middle-temperature area have increased. In terms of space, the high-temperature area of Huadu District, Guangzhou, is mainly distributed in the built-up area in the south and north of the city; the sub-low temperature area is distributed on the edge of the built-up area; the medium-temperature area occupies most of the district of Huadu District, distributed in the city's central area and the edge of the low-temperature area; and the low-temperature area is distributed in the water body and dense vegetation area.



Keyword— Atmospheric Correction Method; Surface Temperature Inversion; Urban Heat Island (UHI); Spatio-temporal Evolution, Normalized Difference Vegetation Index (NDVI)

I. INTRODUCTION

The urban heat island (UHI) effect refers to the phenomenon that the temperature in the city is significantly higher than that in the outer suburbs due to a large number of artificial heating systems, the increase of high heat storage bodies such as buildings and roads, the decrease of green space, and the decrease of wind speed affecting heat transport. The measure of its strength is heat island intensity. Human beings have long discovered that

the atmospheric environment in cities has different characteristics from those in rural and mountainous areas. The British man Lake Howard first documented in 1833 the phenomenon of higher temperatures in the center of London compared to the suburbs, and Manley first proposed the concept of Urban Heat Island (UHI) in 1958. It is now widely believed that the urban heat island effect refers to the phenomenon where, when a city develops to a certain scale, the temperature of the city is significantly

higher than that of the suburbs due to changes in the nature of the urban underlying surface, air pollution, and the emission of artificial waste heat, forming a phenomenon similar to high-temperature islands.

With the rapid urbanization process and the rapid expansion of urban built-up areas, the urban heat island effect is intensifying. Materials such as asphalt, concrete, and cement transform natural surfaces into the underlying surface of the building, reducing transpiration rates, rainwater retention, and altering the reflectivity of the surface [1], "resulting in undesirable thermal effects." Urban land absorbs solar radiation during the day and slowly re-radiates the absorbed heat at night. This results in the generation of heat islands in urban areas, with higher temperature values compared to neighboring areas [2]. During the year, the increase in summer surface temperature contributes to the increase in atmospheric temperature, which seriously affects the comfort of the human body surface. The severe haze weather in winter will also have a synergistic effect with the heat island effect, leading to the deterioration of the winter environment.

Huadu District of Guangzhou is located in the central part of Guangdong Province, the north of the Pearl River Delta, and the north of Guangzhou, Guangdong Province. In 2021, the main goal of the economic and social development of Huadu District in the next five years is to

achieve an average annual GDP growth rate of about 6% and build a new industrial pattern of "one core leading, three belt linkages, and six functional areas supporting." Under the grand goal of rapid construction and harmonious rise, the expansion of urban scale will accelerate, and the heat island effect will be particularly significant. Therefore, studying the spatio-temporal evolution characteristics of the heat island effect in Huadu District of Guangzhou has important theoretical and practical significance for the protection of the urban geological environment, disaster prevention and reduction, and the realization of sustainable urban development.

II. STUDY AREA AND DATA SOURCE

2.1 Study Area

Huadu District is located in the north of Guangzhou. Its climate is a subtropical monsoon climate. It has the climatic characteristics of high temperatures, high precipitation, long summers and short winters, and a long frost-free period. The average annual temperature is 21.8 degrees, the average annual rainfall is 1753.9 mm, the average relative humidity is 76%, the dominant wind direction is southeast throughout the year, the frost-free period is 365 days, and the groundwater level is about 1.2–3.5 meters. There are obvious seasonal changes in temperature, humidity, precipitation, wind direction, and wind speed [3] (Figure 1).

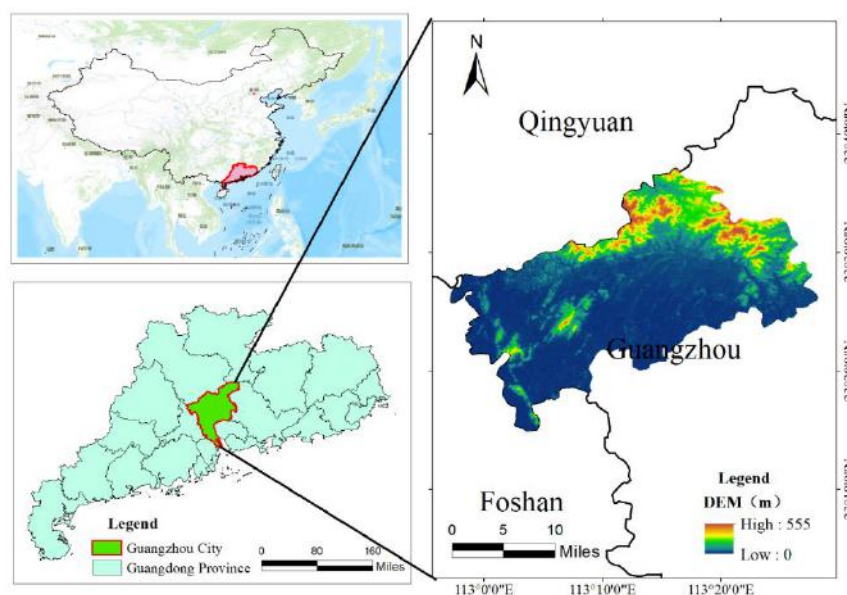


Fig.1 Location and Topographic Map of Huadu District in Guangzhou

2.2 Data Sources

This paper takes the Huadu District of Guangzhou (E113°13'13", N23°24'14") as the research object. The data is obtained from a geospatial data cloud (<http://www.Gscloud.cn>) with good image quality and basically no cloud. Use two Landsat 8 images from the winter of 2013 and 2021 for analysis and comparison

(Table 1). Landsat8 is the eighth satellite of the United States Land Satellite Program (Landsat), launched on February 11, 2013, initially known as the Landsat Data Continuity Mission (LDCM). Landsat 8 carries an Operational Land Imager (OLI) and Thermal Infrared Sensor (TIRS), and many studies on surface temperature inversion use this satellite image data.

Table 1 Remote sensing image data sources

Item	Imagery	
Date	2013-12-31	2021-02-20
Data identification	LC81220442013365LGN01	LC81220442021051LGN00
Sensor type	Landsat8_OLI and TIRS	
Spatial resolution	OLI 30m/ TIRS 100 m	
Strip number	122	
Line number	44	

III. RESEARCH METHODS AND PROCESSES

This study adopts the remote sensing surface temperature inversion method, and the main principle is that after the solar radiation reaches the surface, part of the radiation energy is reflected, and the other part of the energy is absorbed by the ground, so that the ground temperature rises and then is measured by the instrument. At present, the use of remote sensing technology to retrieve land surface temperature has become mainstream; it has a lot of advantages, and the main land surface temperature inversion algorithms are as follows: atmospheric correction method, single window algorithm, and split window algorithm [4].

In this paper, the atmospheric correction method is used to invert the surface temperature of Huadu District. The atmospheric correction method, also known as the radiative transfer equation method, is based on the principle of subtracting the influence of the atmosphere on the surface radiation from the total thermal radiation received by the satellite sensor and converting the

remaining radiation value into the corresponding surface temperature. The heat radiation value of the atmosphere, the energy reflected by the atmosphere down to the sensor through the surface, and the energy transmitted to the sensor through the atmosphere after the surface absorption constitute the total heat radiation of the satellite [5]. The advantage of the radiative transfer equation is that there is no limit to the thermal infrared band, but it needs four parameters: atmospheric transmittance, atmospheric up-going radiation value, atmospheric down-going radiation value, and surface-specific emissivity.

Based on the above principles, this study uses Landsat 8 images as materials. After image preprocessing, NDVI (Normalized Difference Vegetation Index) extraction, vegetation coverage calculation, and surface radiance calculation are performed. Combined with the 10th band image, radiance calculation and temperature inversion are performed. Finally, the spatiotemporal changes are analyzed, and the conclusion is estimated (Figure 2).

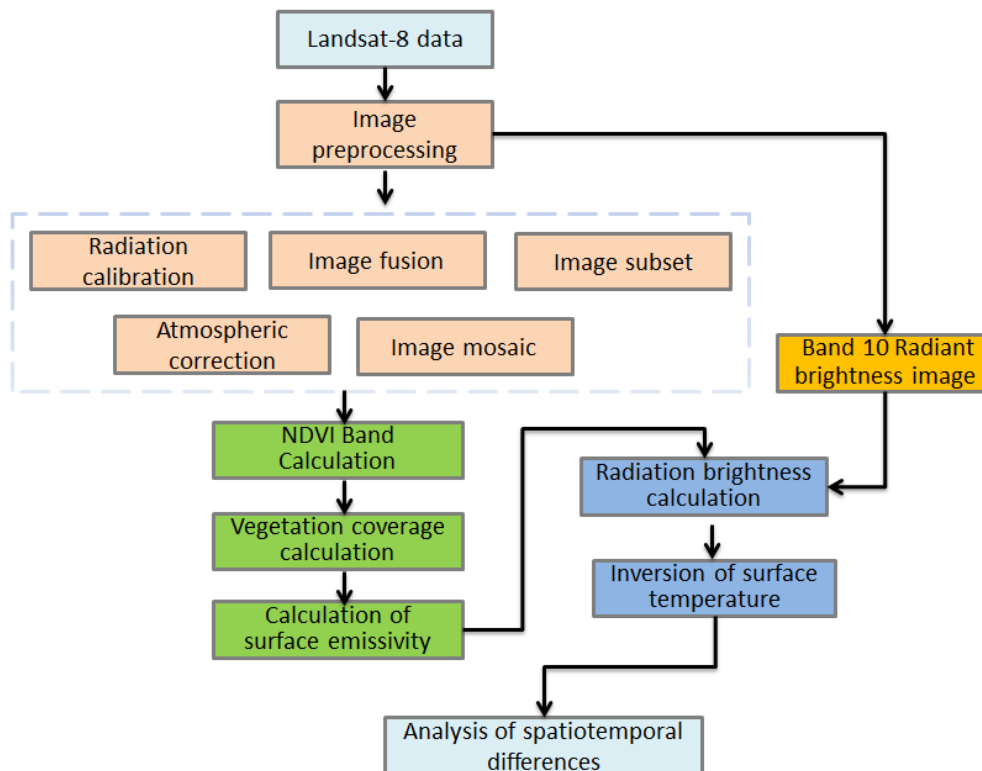


Fig.2 Technical roadmap

3.1 Radiometric Calibration

The surface radiation brightness and surface temperature in the thermal infrared band cannot be directly recorded by the satellite sensor, which is usually stored as a gray value (DN value), and the DN value recorded by the sensor needs to be converted to obtain the actual spectral information of the ground object. We call this conversion process radiation calibration^[6]. Usually, a linear relation is used to complete the conversion of the gray value and the radiation brightness value of ground objects, and the formula is as follows:

$$L_a = \text{Gain} * \text{DN} + \text{Offset} \quad (1)$$

In the formula, L represents the radiation brightness value of the ground object, and its unit is $W/(m^2 \cdot \mu m \cdot sr)$. Gain is the transformation value, and its calculation formula is as follows:

$$\text{Gain} = (L_{\max} - L_{\min}) / 2552.2 \quad (2)$$

In the formula, L_{\max} represents the maximum radiation luminance value, and L_{\min} represents the minimum radiation luminance value. Offset is the deviation transform value, $\text{offset} = L_{\min}$, and the calibration

parameters are obtained from the Landsat image metadata to calculate the radiometric calibration data by selecting high-gain bands.

3.2 Calculation of NDVI

The formula for NDVI is $(NIR - R) / (NIR + R)$ (3).

NIR is the reflection value in the near-infrared band. R is the reflection value in the red light band. The NDVI is one of the important parameters reflecting crop growth and nutritional information. Based on this parameter, the nitrogen demand of crops in different seasons can be determined, which plays an important guiding role in the rational application of nitrogen fertilizer.

1. The application of NDVI: detecting vegetation growth status, vegetation coverage, and eliminating some radiation errors;
2. -1 visible light high reflection; 0 represents the presence of rocks or bare soil, and NIR and R are approximately equal; A positive value indicates vegetation coverage and increases with increasing coverage.
3. The limitation of NDVI is that it enhances the contrast

between NIR and R reflectivity through nonlinear stretching. For the same image, when calculating RVI and NDVI separately, it can be found that the rate of increase in RVI value is higher than that of NDVI, indicating that NDVI has a lower sensitivity to high vegetation areas.

This study with the NDVI of the ENVI Toolbox, select the cut multi-spectral OIL band data and calculate the NDVI by using the short red and near infrared bands corresponding to the 4th and 5th bands of OLI in the NDVI calculator parameters dialog box.

3.3 Calculate the Vegetation Coverage

Vegetation coverage reflects the density of vegetation in a region and is also an important parameter of ecological environment assessment. The minimum value of

vegetation coverage is 0, and the maximum value is 1. The inversion formula is as follows:

$$VFC = (NDVI - NDVI_{soil}) / (NDVI_{veg} - NDVI_{soil}) \quad (4)$$

($NDVI_{soil}$ represent the NDVI value of bare land, and $NDVI_{veg}$ represents the NDVI value of pure vegetation cover.)

The above two values are determined according to the actual situation of this paper. For example, the confidence range of 5%~95% is adopted, and VFC_{max} and VFC_{min} are estimated according to experience. Tool input (($b1 \text{ lt } NDVI_{soil}$)*0 + ($b1 \text{ gt } NDVI_{veg}$)*1 + ($b1 \text{ ge } NDVI_{soil}$ and $b1 \text{ le } NDVI_{veg}$)* ($b1 - NDVI_{soil}$)/($NDVI_{veg} - NDVI_{soil}$)[⁷]. Using ENVI's band math, the $NDVI_{soil}$ and $NDVI_{veg}$ values are obtained (Table 2).

Table 3 NDVI values of bare land and pure vegetation

Year	2013	2021
$NDVI_{soil}$	-0.145098	-0.082353
$NDVI_{veg}$	0.364706	0.317647

3.4 Calculation of Specific Emissivity

Surface-specific emissivity is an important parameter of land surface temperature inversion that directly determines the accuracy of the inversion results. In order to obtain more accurate inversion results, this paper uses the surface-specific emissivity algorithm to divide the surface into water bodies, natural surfaces, and urban areas. The specific emissivity of the water body is equal to that of the black body (0.995), and the specific emissivity of the

natural surface and urban area is calculated as follows [⁸]:

$$\text{Natural surface-specific emissivity: } \epsilon_{\text{surface}} = 0.9625 + 0.0614FV - 0.0461FV \quad (5)$$

$$\text{Urban area-specific emissivity: } \epsilon_{\text{building}} = 0.9589 + 0.086FV - 0.0671FV \quad (6)$$

3.5 Estimation of Atmospheric Parameters

The radiation parameter information of Huadu District in 2013 and 2021 can be obtained from the NASA website as follows (Table 4):

Table 5 Radiation parameter information

Year	Atmospheric transmittance	Atmospheric upward radiance	Atmospheric downward radiation brightness
2013	0.93	0.50	0.85
2021	0.82	1.34	2.22

3.6 Calculation of Blackbody Radiance

Surface brightness temperature refers to the temperature of the blackbody with the same radiation brightness as the surface, referred to as the surface brightness temperature. That is, the radiation temperature of the surface object

itself is the radiation intensity observed by the sensor at the height of the satellite. Surface brightness temperature can be calculated by the formula

$$D(t) = [Q - q2 - a(1-x)q1] / ax \quad (7)$$

which is converted to Bandmath as follows:

$$(b2-q2-a*(1-b1)*q1)/(a*b1) \quad (8)$$

b1 in the formula is the surface specific emissivity, b2 refers to the radiation brightness value of the 10th band obtained at the beginning, and then the inversion is obtained according to the transmittance a of the atmosphere in the thermal infrared band, the atmospheric upward radiation brightness q2, and the atmospheric downward radiation brightness q1.

3.7 Inversion of Surface Temperature

The true surface temperature can be obtained by the Planck function, as follows:

$$T_s = K2 / \ln(K1 / B(T_s) + 1) \quad (9)$$

Where, T_s is the true surface temperature, $K1$ and $K2$ are constants, and the values of $K1$ and $K2$ are different for different sensors. The specific values of $K1$ and $K2$ are shown in the Table 4 [4]:

Table 6 Different sensor K1, K2 value standard

Sensor type	K1	K2
Landsat8_OLI	774.89	1321.08
Landsat7_ETM+	666.09	1282.71
Landsat5	607.76	1260.56

IV. ANALYSIS RESULT

4.1 Divide Urban Heat Island Effect Areas

Due to the different imaging times of remote sensing images, the difference between the maximum and minimum values of the inverted land surface temperature is large, and the existence of abnormal temperature values is not convenient for comparative analysis, so the images are normalized. The current normalization method is normalized according to the maximum and minimum values, which is not suitable for the division of heat islands in the region due to the existence of outliers and the accidentality of this method, and the other method is to normalize the mean-standard deviation. In this paper, the

mean-standard deviation method was used to statistically analyze the heat island effect. The study area is divided into five temperature range classes, and the mean-standard deviation classification rules and heat island classification are shown in Table 5[9].

According to the above principles, after reclassification, the heat island of surface temperature is divided into five levels, including the low-temperature areas, sub-low temperature area, middle-temperature area, sub-high temperature area, and high-temperature area. Meanwhile, we complete the visualization of surface temperature classification zoning maps for 2013 and 2021 (Figure 3 and Figure 4).

Table 7 Mean-standard deviation temperature classification

Heat island level	Temperature zone level	The difference in average temperature between urban core and non-core areas
Cold island	Low temperature area	$T_s < \mu - \text{std}$
Green Island	sub-low temperature area	$\mu - \text{std} \leq T_s < \mu - 0.5\text{std}$
Normal area	Middle-temperature area	$\mu - 0.5\text{std} \leq T_s \leq \mu + 0.5\text{std}$
Subheat island	Sub-high temperature area	$\mu + 0.5\text{std} < T_s \leq \mu + \text{std}$
Island of intense heat	High-temperature area	$T_s > \mu + \text{std}$

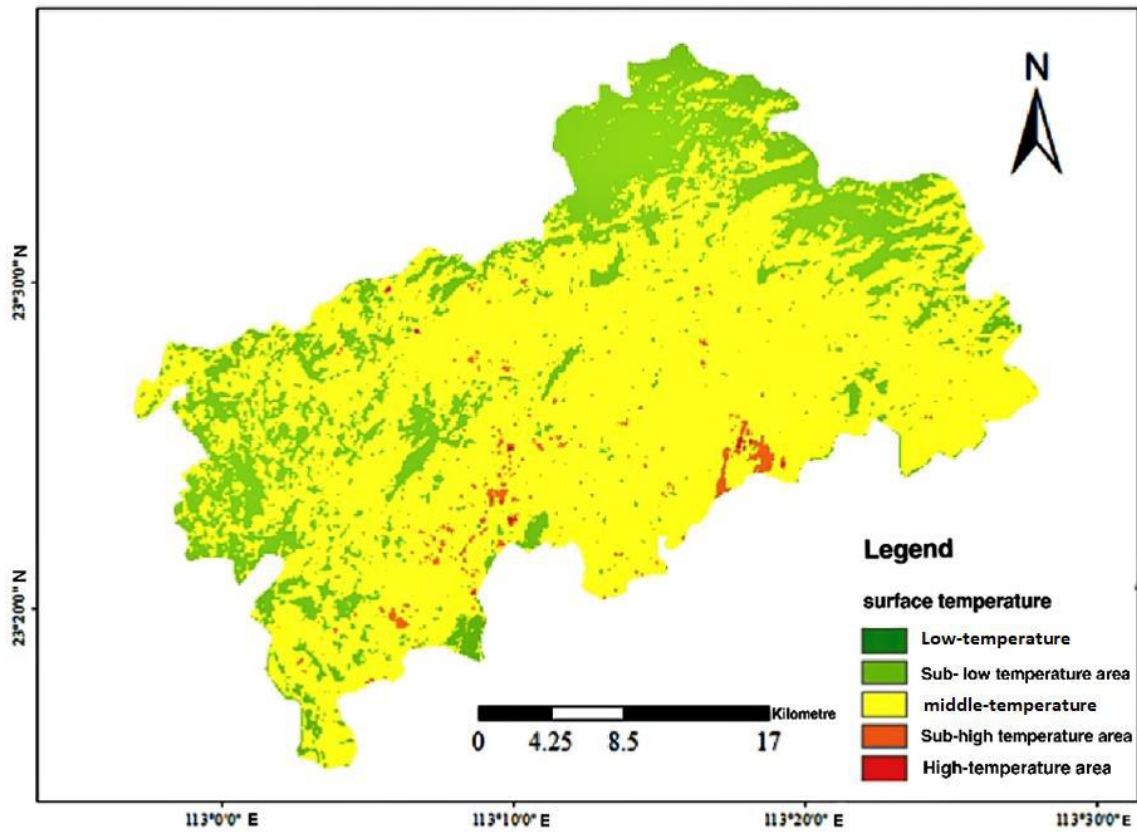


Fig.3 Classification map of surface temperature in Huadu district in 2013

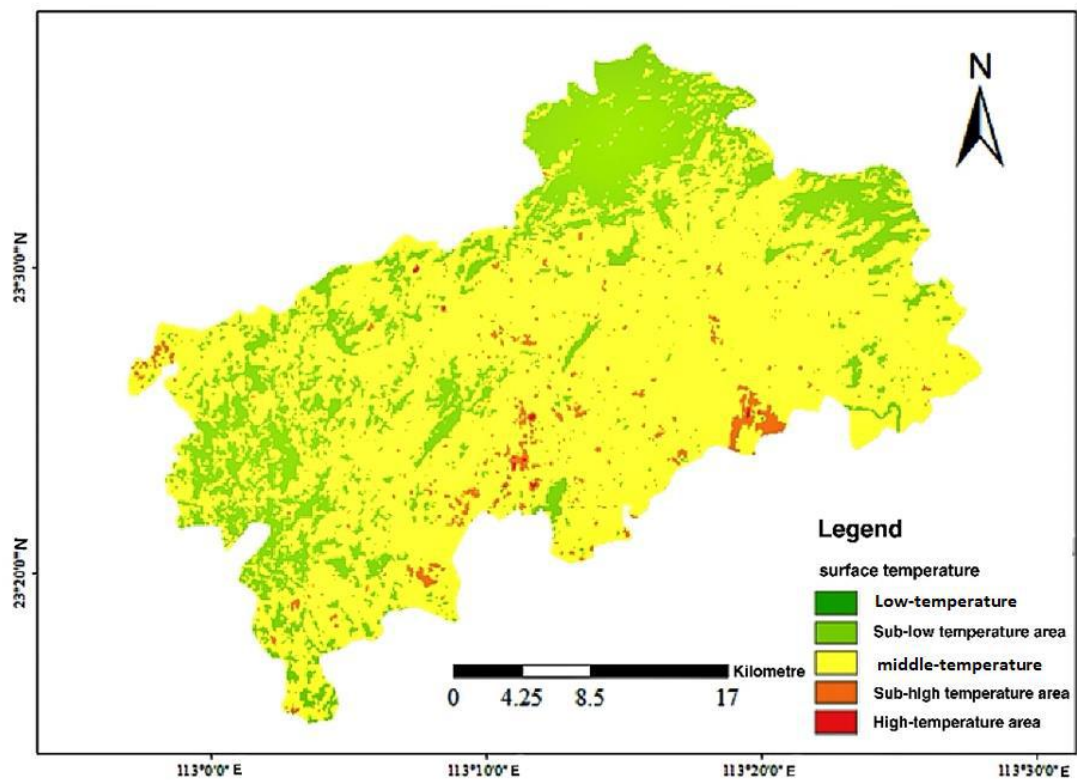


Fig.4 Classification map of surface temperature in Huadu district in 2021

4.2 Analysis of Spatio-temporal Changes of Heat Island Effect

Due to the different imaging times of remote sensing images, the difference between the maximum and minimum values of land surface temperature and the existence of abnormal temperature values are not accurate for comparative analysis. However, it can still provide a reference value for recognizing the trending patterns in the difference in temperature change. From the analysis results, the intense heat island area of Huadu District in 2013 and 2021 was located in the southern part of the city (Figure 5 and Figure 6), and distributed in built-up areas. The sub-heat island area is distributed along the edge of the high-temperature area, and there is no obvious rule. Normal areas and middle-temperature areas occupy most

of the whole urban area of Huadu District and are mostly distributed in the surrounding areas of Huadu District. Low-temperature areas are mainly distributed in water areas, lakes, rivers, and other low-temperature areas.

Overall, the spatial distribution of urban heat islands in Huadu District has clearly changed in the past 8 years. The area of the strong heat island area has increased and expanded along the northern and eastern parts of the city, while the area of the sub-heat island area has decreased and shifted to the high-temperature area, while the distribution of the normal area and the green island area has not changed greatly. However, most of the low-temperature areas in the western part of Huadu District have been transformed into sub-low temperature areas and medium temperature areas.

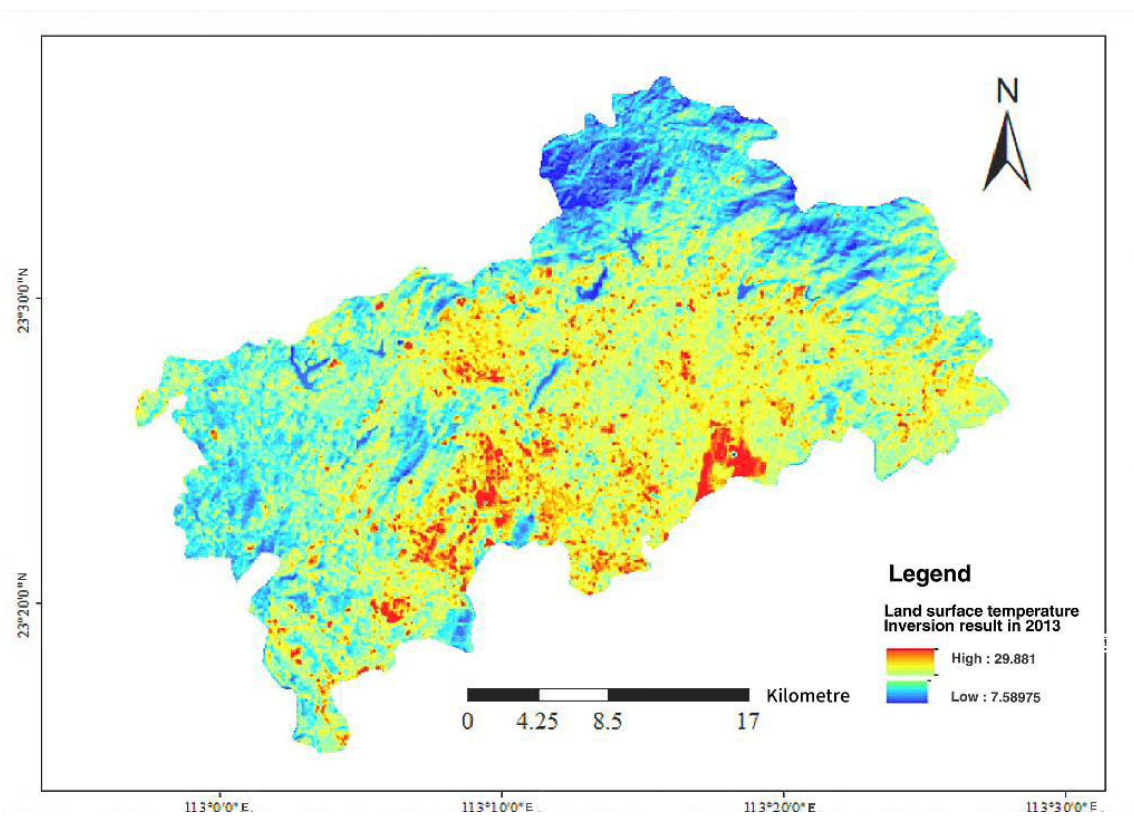


Fig.5 Inversion results of surface temperature in Huadu, Guangzhou in 2013

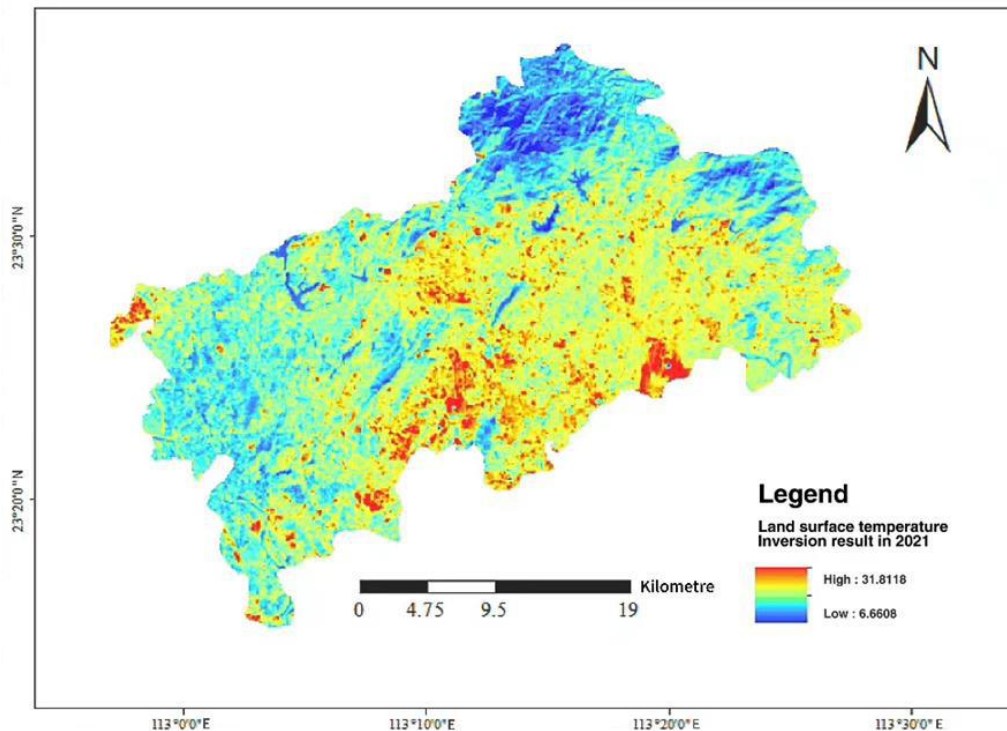


Fig.6 Inversion results of surface temperature in Huadu, Guangzhou in 2021

V. CONCLUSIONS

In terms of spatio-temporal analysis of land surface temperature, it is found that the urban intense heat island area of Huadu District is distributed in the south and east, and the small built-up area is in the northwest. The sub-low temperature area has no obvious distribution pattern, and most of them are located at the edge of the middle-temperature area. The sub-low temperature area and low-temperature area occupy a small part of Huadu District and are distributed in the northern fringe area, while the low-temperature area is distributed in the water body and the lush vegetation area. In the past 8 years, the strong hot island area has shown an expanding trend along the east-west direction of the parallel.

The increase in building area is the main reason leading to the expansion of the strong heat island area, and water and vegetation are the main factors leading to the decline of the heat island effect. Therefore, urban construction should be rationally planned, and the protection of vegetation areas should be strengthened in the process of urbanization. According to research, if the urban green coverage rate is greater than 30%, the heat island effect can be significantly

alleviated. The coverage rate is greater than 50%, and the mitigation effect of green space on heat island is extremely significant. In addition, roof greening also has a certain effect on improving the urban climate. Every inch of urban land is valuable. The popularization of roof greening can effectively increase the urban green area and play a role in heat insulation and rainwater storage. At the same time, it is suggested to increase the area of urban water bodies and wetlands. Urban water bodies and wetlands have a huge heat capacity and are a cold source in summer, which can absorb a lot of waste heat from the urban environment.

The change in urban surface albedo is also an important cause of urban heat islands. Improving urban reflectivity can reflect part of solar radiation outward, reduce urban heat transfer to solar radiation, and alleviate the urban heat island effect. Therefore, in the process of urban planning and design, materials with high reflectivity are selected or the building surface is painted so that more solar radiation is reflected out of the urban space. For example, the use of light-colored materials on roofs, roads, parking lots, etc. can effectively slow down the urban heat island effect^[10]. Chicago, USA, has strengthened albedo management in

urban planning and developed building codes to improve roof reflectivity, which has proved to be beneficial to alleviate the urban heat island effect.

In addition, in recent years, the construction thinking of sponge cities has also become an important strategy for future urban development. It is a concept that promotes green building construction, low-carbon city development, and the formation of innovative ecological environments in smart cities. It is also an organic combination of modern green technologies and various factors such as society, environment, and culture in the context of the characteristics of the new era.

ACKNOWLEDGEMENTS

The author is grateful for the research grants given to Ruet-Yuan Wang from GDUPT Talents Recruitment (No.2019rc098), Peoples R China under Grant No.702-519208, and Academic Affairs in GDUPT for Goal Problem-Oriented Teaching Innovation and Practice Project Grant No.701-234660.

REFERENCES

- [1] Voogt, J. A., Oke, T. R., Thermal remote sensing of urban climates[J]. *Remote Sensing of Environment*, 2003, 86(3):370-384.
- [2] Cao, C., Li, X. H., Zhang, M., et al. Correlation analysis of the urban heat island effect and its impact factors in China[J].*Environmental Science*, 2017, 38(10):3987-3997.
- [3] Huang, T. L., Liu, H. Z., and Ke, J. C. Study on characteristics of urban heat island effect in Guangzhou based on Landsat TM satellite data. *Beijing Surveying and Mapping*, 2018, 32(8):891-896.
- [4] Wang, D. D., Wan, A. G., and Tong, Z. H. Spatial and temporal evolution of urban heat island effect in Nanjing City based on Landsat data. *Jiangxi science*, 2020, 42 (5): 705-709. The DOI: 10.13990 / j.issn1001-3679.2020.05.017.
- [5] Wang, Q. M., Spatial and temporal distribution of urban heat island effect in Changchun based on remote sensing technology. Changchun: Changchun Institute of Technology, 2018.
- [6] Ye, B. Spatiotemporal evolution characteristics of urban

heat island effect in Nanchang City based on Landsat satellite images. Guilin University of Technology, 2019. DOI: 10.27050 / dc.nki.GGLGC.2019.000002.

- [7] Jia, W. H., Lian, L. M., and Lv, Y. P. Vegetation coverage extraction in Yellow River Delta based on TM data. *Geographical Information World*, 2012(6): 62-66+74.
- [8] Qin, Z. H., Li, W. J., Xu, B., Chen, Z., and Liu, J. Estimation of land surface specific emissivity in Landsat TM6 band. *Remote Sensing for Land and Resources* 2004, 16(3):28-32
- [9] Wu, H. F., and Chen, Z. Q. Temporal and spatial evolution of urban heat island effect in Fuzhou. *Journal of Tangshan Teachers University*, 2018, 40(06):155-160. (in Chinese)
- [10] Huang, T. L., Luo, J., Ke, J. C., and Wang, X. Spatio-temporal heat island effect in Pearl River Delta urban agglomerations based on multi-source remote sensing data Surveying and mapping, evolution characteristics. *Journal of Beijing* 2019 (10): 1165-1170. The DOI: 10.19580 / j.carol carroll nki.1007-3000.2019.10.011.